DOI: 10.1002/asia.200700264

Cobalt Hydroxide Nanosheets and Their Thermal Decomposition to Cobalt Oxide Nanorings

Xiaohe Liu,*[a] Ran Yi,[a] Ning Zhang,[a] Rongrong Shi,[a] Xingguo Li,[b] and Guanzhou Qiu*[a]

Abstract: We demonstrate herein that single-crystalline β-cobalt hydroxide (β-$Co(OH)_2$) nanosheets can be successfully synthesized in large quantities by a facile hydrothermal synthetic method with aqueous cobalt nitrate as the cobalt source and triethylamine as both an alkaline and a complexing reagent. This synthetic method has good prospects for the future large-scale production of single-crystalline β-$Co(OH)_2$ nanosheets owing to its high yield, low cost, and simple reaction apparatus. Single-crystalline porous nanosheets and nanorings of cobalt oxide (Co_3O_4) were obtained by a thermal-decomposition method with single-crystalline β-$Co(OH)_2$ nanosheets as the precursor. A probable mechanism of formation of β-$Co(OH)_2$ nanosheets, porous Co_3O_4 nanosheets, and Co_3O_4 nanorings was proposed on the basis of the experimental results.

Keywords: cobalt · hydrothermal synthesis · nanorings · nanosheets · nanostructures

Introduction

Cobalt hydroxide has attracted increasing attention in recent years because of its novel electric and catalytic properties and important technological applications.[1–3] In particular, cobalt hydroxide can be used to enhance electrochemical performance when added to nickel oxyhydroxide electrodes (NOEs) by enhancing the electrode conductivity and chargeability.[4] It is well known that cobalt hydroxide has two polymorphs: α- and β-$Co(OH)_2$. These two phases are all-layered and have the same hexagonal structures, except that the β form is isostructural with brucite-like compounds and consists of a hexagonal packing of hydroxy ions with Co^{II} occupying alternate rows of octahedral sites.[5] α-$Co(OH)_2$, however, is isostructural with hydrotalcite-like compounds that consist of stacked $Co(OH)_{2-x}$ layers intercalated with various anions (e.g., nitrate, carbonate, etc.) in the interlayer space to restore charge neutrality. α-$Co(OH)_2$ thus has a larger interlayer spacing (>7.0 Å, depending on the intercalated anions) than the brucite-like β-$Co(OH)_2$ (4.6 Å); because of that, the α form has higher electrochemical activity. However, the hydrotalcite-like phase (α-$Co(OH)_2$) is metastable and easily undergoes a phase transformation into the more stable brucite-like compounds in strongly alkaline media. β-$Co(OH)_2$ is often selected as additives of alkaline secondary batteries owing to its stability in alkaline electrolytes and enhanced conductivity when charged to β-CoOOH.[6,7]

Several chemical and electrochemical methods have been employed to prepare cobalt hydroxide, for example, forced precipitation of $Co(NO_3)_2$, direct precipitation with liquid ammonia[8] and potassium hydroxide,[9] urea hydrolysis,[10] and electrochemical synthesis.[11] Sampanthar and Zeng[12] reported the synthesis of butterfly-like β-$Co(OH)_2$ nanocrystals by the ethylenediamine-mediated approach. Li et al.[13] prepared β-$Co(OH)_2$ nanostructures consisting of a mixture of nanoflakes and nanorods by the $CoC_2O_4{\cdot}2H_2O$ conversion method. Recently, Liu et al.[14] synthesized single-crystalline nanosheets of α- and β-$Co(OH)_2$ by using hexamethylenetetramine as a hydrolysis agent. Hou et al.[15] also synthesized single-crystalline β-$Co(OH)_2$ nanosheets by homogeneous precipitation with sodium hydroxide as the alkaline reagent in the presence of poly(vinylpyrrolidone). Although

[a] Dr. X. Liu, R. Yi, N. Zhang, R. Shi, Prof. Dr. G. Qiu
Department of Inorganic Materials
Central South University
Changsha, Hunan 410083 (China)
Fax: (+86) 731-8879815
E-mail: liuxh@mail.csu.edu.cn
qgz@mail.csu.edu.cn

[b] Prof. Dr. X. Li
College of Chemistry and Molecular Engineering
Peking University, Beijing 100871 (China)

Supporting information for this article is available on the WWW under http://www.chemasianj.org or from the author.

many attempts have been made on the synthesis of cobalt hydroxides, the control of their morphology, size, and crystallinity still remains a highly sophisticated challenge to materials scientists and chemists.

Spinel cobalt oxide (Co_3O_4) is an important magnetic p-type semiconductor that has been demonstrated to have considerable application as, for example, solid-state sensors, ceramic pigments, heterogeneous catalysts, rotatable magnets, electrochromic devices, and in energy storage.[16–19] Several methods have been successfully applied to the synthesis of Co_3O_4 nanoparticles, such as spray pyrolysis, chemical vapor deposition, sol–gel techniques, forced hydrolysis, and so on.[20–23] Recently, a variety of novel shapes such as Co_3O_4 nanoboxes,[24] nanocubes,[25] nanofibers,[26] nanorods,[27] and nanotubes[28] have been reported. However, as far as we know, there is no study on the preparation of Co_3O_4 nanorings until now.

Herein we demonstrate that single-crystalline β-$Co(OH)_2$ nanosheets can be successfully synthesized in large quantities by a facile hydrothermal synthetic method with triethylamine as both an alkaline and complexing reagent under mild conditions. The influence of hydrothermal temperature, reaction time, amount of triethylamine, and concentration of cobalt nitrate on the size and shape of nanosheets was carefully investigated. Single-crystalline porous nanosheets and nanorings of spinel cobalt oxide (Co_3O_4) were successfully obtained by a thermal-decomposition method with single-crystalline β-$Co(OH)_2$ nanosheets as the precursor. The mechanism of formation of porous nanosheets and nanorings of Co_3O_4 is also discussed on the basis of the experimental results. Notably, the current synthetic strategy can be used to synthesize other metal hydroxide nanosheets and prepare corresponding metal oxide nanorings by calcination at appropriate temperatures, and it has good prospects for future large-scale applications owing to its high yields, simple reaction apparatus, and low reaction temperature.

Results and Discussion

X-ray diffraction (XRD) was carried out to determine the chemical composition and crystallinity of the as-prepared products. Figure 1 shows typical XRD patterns of β-$Co(OH)_2$ nanosheets prepared by using a 1.5-mL solution of triethylamine at 180 °C for 24 h. All diffraction peaks in this pattern can be indexed to the hexagonal cell of brucite-like β-$Co(OH)_2$ with lattice constants $a = 3.182$ and $c = 4.658$ Å (space group: $P\bar{3}m1$ (No. 164)), which are consistent with the values in the literature (JCPDS 30-0443). The (001) peak is taller and far narrower than other peaks in the reflections, which implies the highly preferentially oriented growth of the β-$Co(OH)_2$ nanosheets. Diffraction peaks of α-$Co(OH)_2$ or impurities were not observed, which indicates the high purity of the final products successfully synthesized under the current experimental conditions.

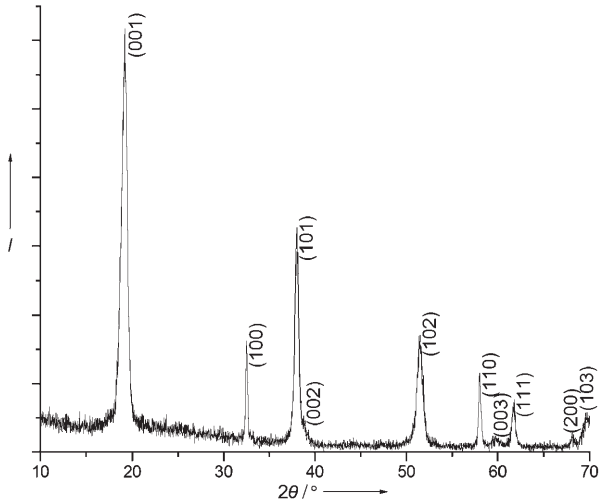

Figure 1. XRD pattern of the as-prepared β-$Co(OH)_2$ nanosheets obtained by using 1.5 mL triethylamine at 180 °C for 24 h.

The size and morphology of the as-prepared product were examined by scanning electron microscopy (SEM) and transmission electron microscopy (TEM). The SEM images (Figure 2a) indicate that a large quantity of hexagonal β-$Co(OH)_2$ nanosheets with good uniformity were achieved by using this approach. These nanosheets had a mean width of about 120 nm with little deviation. The inset shows a high-magnification SEM image. Here, the corners and edges of the β-$Co(OH)_2$ nanosheets can be clearly observed. The average thickness and edge size of these hexagonal nanosheets are about 15 and 60 nm, respectively. SEM observations also indicated that almost 100% of the as-prepared products are uniform hexagonal β-$Co(OH)_2$ nanosheets. Figure 2b is the representative TEM image, in which the β-$Co(OH)_2$ nanosheets are hexagonal and quasi-hexagonal with angles of adjacent edges of 120° and widths in the range 100–170 nm. The inset of Figure 2b shows the selected area electron diffraction (SAED) pattern of the β-$Co(OH)_2$ nanosheets, which reveals that the β-$Co(OH)_2$ nanosheets are single-crystalline hexagonal structures lying on their {001} crystal planes, consistent with the XRD result presented above.

High-resolution transmission electron microscopy (HRTEM) provided further insight into the nanostructure of the as-prepared hexagonal β-$Co(OH)_2$ nanosheets. Fig-

Abstract in Chinese:

本研究通过便利的水热反应合成了的单晶 β-$Co(OH)_2$ 纳米片，采用 X 射线衍射（XRD）、扫描电子显微镜（SEM）、透射电子显微镜（TEM）和高分辨透射电子显微镜（HRTEM）对 β-$Co(OH)_2$ 进行了表征，结果显示所得 β-$Co(OH)_2$ 均为六边形纳米片，其临边夹角为 120°。利用单晶 β-$Co(OH)_2$ 纳米片为前驱在空气中的热分解反应合成了多孔的单晶 Co_3O_4 纳米片和单晶 Co_3O_4 纳米环，并比较了它们的比表面积和电化学性能。研究结果表明多孔的 Co_3O_4 纳米片具有较大的比表面积、较高的可逆比容量和较好的循环稳定性能，多孔的 Co_3O_4 纳米片的可逆容量达 1301 mAh g^{-1}， 21 次循环后比容量仍为 1001 mAh g^{-1}，是有希望的锂离子电池正极材料。

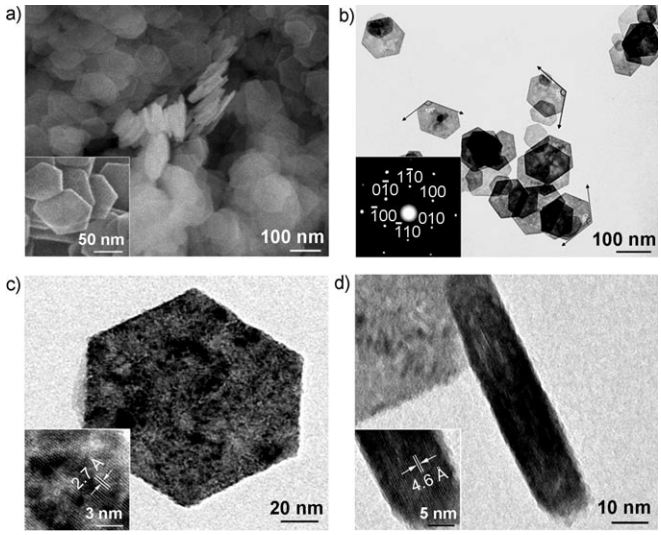

Figure 2. a) Low- and high-magnification (inset) SEM images of the as-synthesized β-$Co(OH)_2$ nanosheets. b) TEM image of the hexagonal β-$Co(OH)_2$ nanosheets with angles of adjacent edges of 120°. Inset: SAED pattern of the β-$Co(OH)_2$ nanosheets taken from an individual hexagonal nanosheet. c) HRTEM image of the individual β-$Co(OH)_2$ nanosheets. d) Side view of the hexagonal β-$Co(OH)_2$ nanosheets. Insets in c) and d): Further-magnified images showing the crystal lattice.

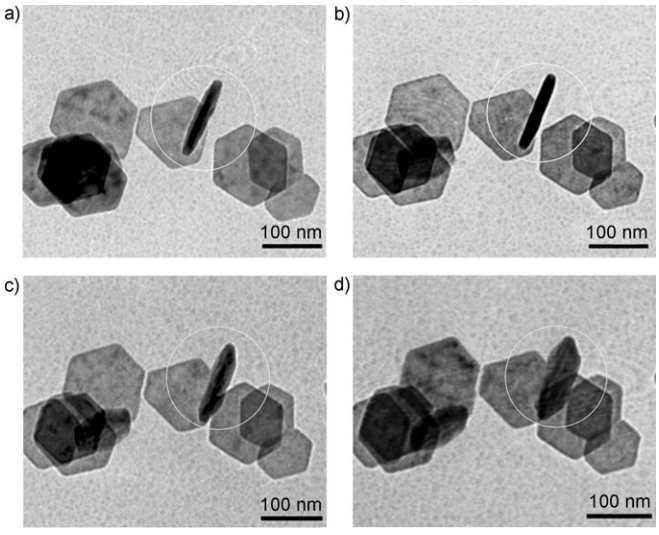

Figure 3. TEM images of the as-prepared β-$Co(OH)_2$ nanosheets observed at different angles: a) −10°, b) 0°, c) 10°, d) 20°.

ure 2c shows a typical image of an individual hexagonal β-$Co(OH)_2$ nanosheet with a mean width of about 120 nm and edge length of about 65 nm. The inset of Figure 2c displays a magnified part of the image. The interlayer spacing was calculated to be about 0.27 nm, which corresponds to the interlayer distance of the (100) crystal plane in β-$Co(OH)_2$. Figure 2d shows a side-view HRTEM image of an individual β-$Co(OH)_2$ nanosheet with a thickness of about 15 nm. The well-resolved lattice fringes in the nanosheet can be clearly observed, which confirms that the nanosheets were formed with a single-crystalline structure. Further magnification clearly shows that the interlayer spacing is about 0.46 nm (Figure 2d, inset), which corresponds to the interlayer distance of the (001) crystal plane of brucite-like β-$Co(OH)_2$ and shows that the growth direction of β-$Co(OH)_2$ is along the (001) crystal plane.

To confirm the morphology of the as-prepared product further, a tilted-angle investigation was carried out to obtain the TEM images from different viewing angles. Some of the nanorod-like β-$Co(OH)_2$ structures were virtually hexagonal nanosheets in shape, as shown by the areas marked with a circle in Figure 3. Figure 3b is a perpendicular view of the β-$Co(OH)_2$ nanocrystals with a perfect rodlike shape. When the copper grid was tilted through −10–20°, parts of the rodlike pattern disappeared, and the hexagonal sheetlike pattern appeared gradually. When it was tilted to 20°, nearly hexagonal nanosheets resulted (Figure 3d). Furthermore, the hexagonal sheetlike pattern can theoretically transform into the rodlike pattern because the two patterns are just a result of the different viewing angles of the same product. Such a transformation can also be clearly seen in Figure 3. This behavior means that the as-prepared products are indeed hexagonal β-$Co(OH)_2$ nanosheets, which agrees well with the SEM results.

Furthermore, further studies suggested that hydrothermal temperature, reaction time, amount of triethylamine, and concentration of cobalt nitrate all influence the size and morphology of β-$Co(OH)_2$ nanosheets. For example, the size of the $Co(OH)_2$ nanosheets was small and the crystallinity was poor at low temperature, whereas the average size and crystallinity of the nanosheets gradually increased with elevation of hydrothermal temperature. Figure 4a shows a typical TEM image of the product prepared at 100 °C over 24 h. Here, the hexagonal and quasi-hexagonal nanosheets can be clearly observed in addition to some nanoparticles. When the reaction temperature was elevated to 140 °C, the final products were mostly made up of nanosheets with widths in the range 60–140 nm (Figure 4b). When the reaction time was decreased to 2 h, the product formed consisted of nanosheets with widths in the range 70–150 nm as well as some nanoparticles with a mean size of 15 nm (Figure 4c). Figure 4d shows the TEM image of products obtained by using a 0.5-mL solution of triethylamine at 180 °C for 24 h, which clearly shows the nanosheets as fine hexagons with widths in the range 100–260 nm. Generally, the size and morphology of the β-$Co(OH)_2$ nanosheets could also be manipulated by changing the concentration of cobalt nitrate. Figure 4e shows the TEM image of products prepared by using 0.5 mmol $Co(NO_3)_2{\cdot}6H_2O$, in which hexagonal $Co(OH)_2$ nanosheets with a mean length of about 100 nm and a thickness of about 10 nm can be clearly observed. Furthermore, a few large nanosheets were also found. When the concentration of cobalt nitrate doubled, that is, when 2 mmol $Co(NO_3)_2{\cdot}6H_2O$ was used, the length and thickness of the hexagonal $Co(OH)_2$ nanosheets were about 150 and 15–20 nm, respectively (Figure 4f). However, further elevation of the cobalt nitrate concentration to five or ten times the original resulted in morphologies of the hexagonal nanosheets that

CHEMISTRY
AN ASIAN JOURNAL

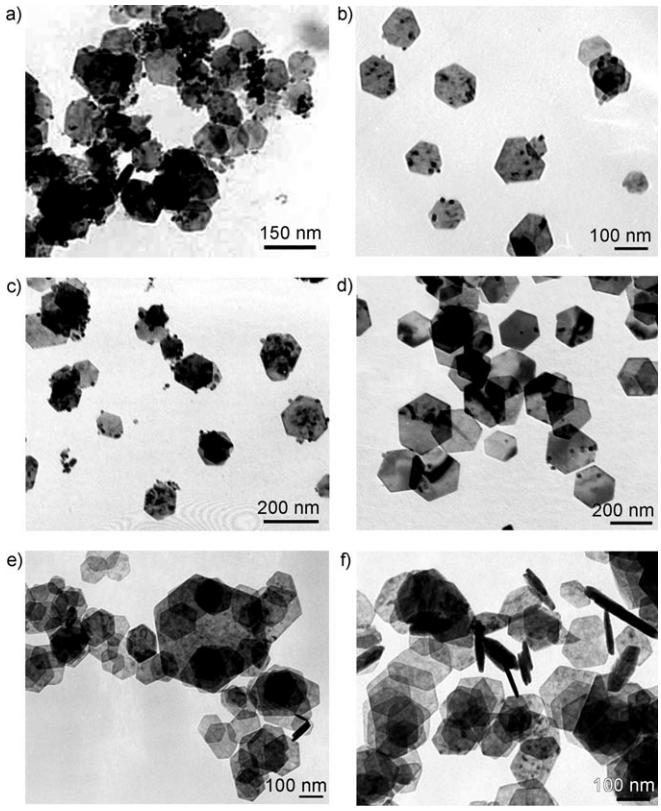

Figure 4. a–c) TEM images of hexagonal β-$Co(OH)_2$ nanosheets synthesized by using 1.5 mL triethylamine at different reaction temperatures and time: a) 100 °C, 24 h; b) 140 °C, 24 h; c) 180 °C, 2 h. d) TEM images of hexagonal β-$Co(OH)_2$ nanosheets synthesized by using 0.5 mL triethylamine at 180 °C for 24 h. e–f) TEM images of hexagonal β-$Co(OH)_2$ nanosheets synthesized by using different cobalt nitrate concentrations at 180 °C for 24 h: e) 0.5 mmol; f) 2 mmol.

tended to be irregular (see Supporting Information, Figures S1 and S2), which implies that the nucleation and growth behavior were out of kinetic control.[29]

The thermal behavior of the hexagonal β-$Co(OH)_2$ nanosheets oxidized to spinel Co_3O_4 was investigated with thermogravimetric analysis (TGA) and differential scanning calorimetry (DSC) in the temperature range 25–800 °C (Figure 5). The gradual mass loss in the range 25–150 °C can be attributed to evaporation of the adsorbed triethylamine and water species on the nanosheet surfaces. The major weight-loss profile exhibits a well-defined decrease between 150 and 400 °C with an inflection point at about 170 °C. The weight loss was measured to be about 13.7% over and above that of the adsorbed triethylamine and water species, in good agreement with the theoretical value (13.6%). The DSC curve shows an endothermic peak at 172 °C, which corresponds to the dominant mass loss.

Cobalt oxide can be obtained by a thermal-decomposition method with cobalt hydroxide as the precursor, on the basis of the TGA and DSC results. Single-crystalline porous nanosheets and nanorings of cobalt oxide (Co_3O_4) were selectively obtained by calcination of as-prepared hexagonal β-$Co(OH)_2$ nanosheets obtained by using a 1.5-mL solution

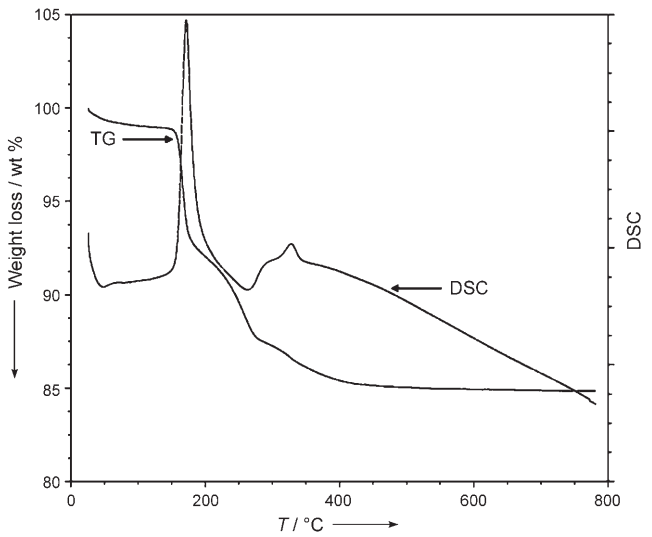

Figure 5. DSC and TGA curves of the hexagonal β-$Co(OH)_2$ nanosheets.

of triethylamine at 180 °C for 24 h in air at 400 and 600 °C, respectively, for 2 h. Figure 6 shows the XRD patterns of the porous Co_3O_4 nanosheets and Co_3O_4 nanorings. All the

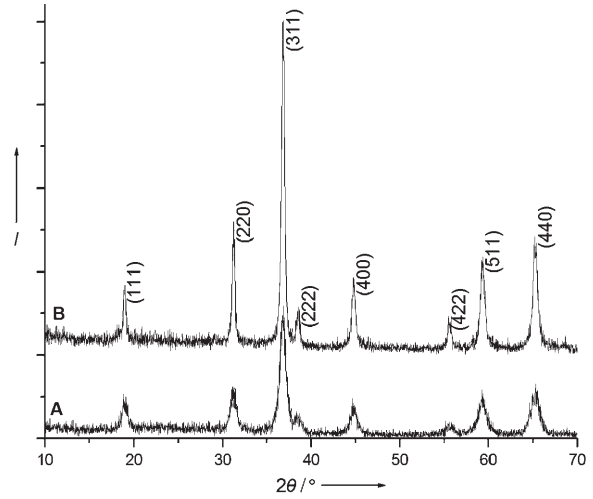

Figure 6. XRD patterns of porous Co_3O_4 nanosheets (A) and Co_3O_4 nanorings (B) obtained by calcination of as-synthesized β-$Co(OH)_2$ nanosheets in air at 400 and 600 °C, respectively, for 2 h.

reflections in the XRD patterns can be indexed to the pure face-centered-cubic phase (space group: *Fd3m* (No. 227)) of spinel cobalt oxide with lattice constant $a = 8.065$ Å (JCPDS 74-1657). No impurity peaks were observed, which indicates that brucite-like $Co(OH)_2$ was completely converted into the spinel structure Co_3O_4 by calcination in air at 400 and 600 °C for 2 h. When the calcination temperature was increased, the diffraction peaks became taller and much narrower, thus showing that the crystallinities of the samples were improved.

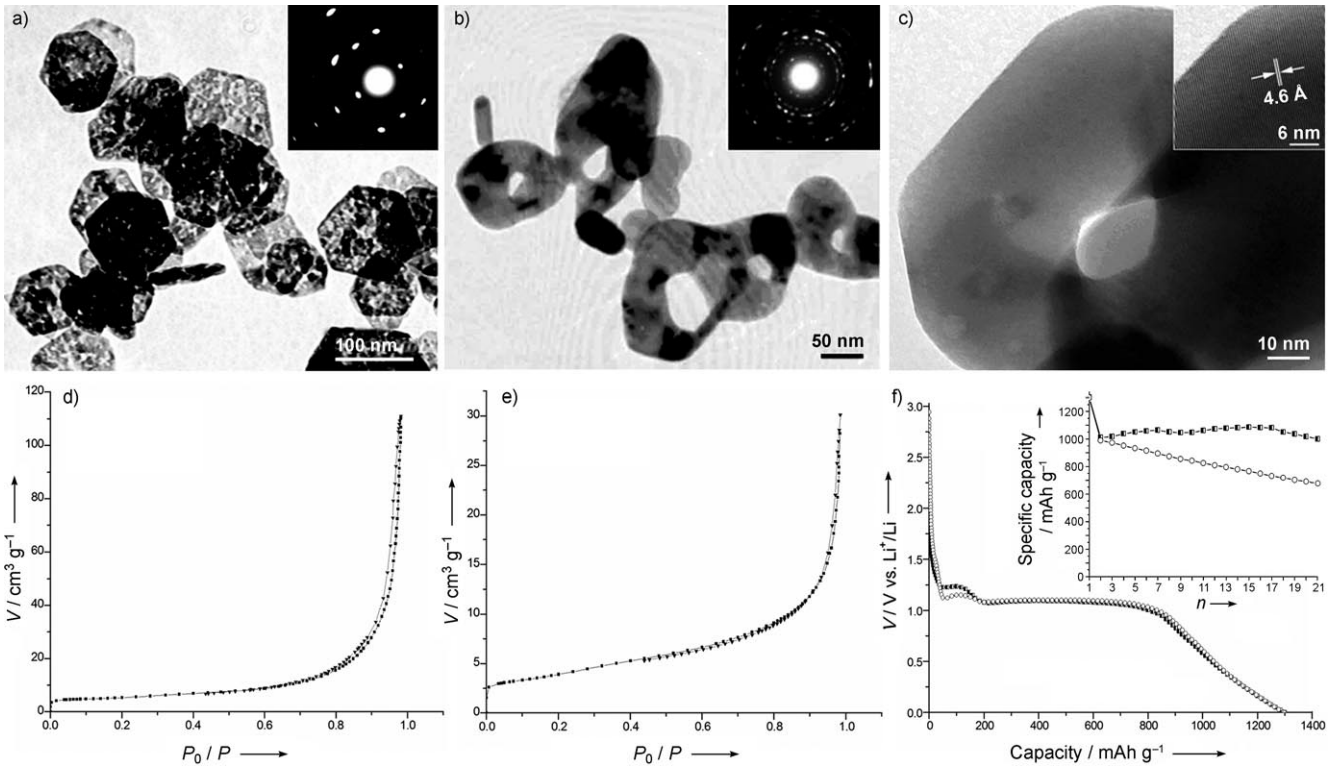

Figure 7. a) TEM image of porous Co_3O_4 nanosheets. Inset: SAED pattern of the porous Co_3O_4 nanosheets taken from an individual nanosheet, which indicates that each porous nanosheet is a single crystal. b) TEM image and SAED pattern (inset) of Co_3O_4 nanorings. c) HRTEM image of an individual Co_3O_4 nanoring. Inset: higher-magnification image of Co_3O_4 nanoring obtained from a selected area in c). d) and e) N_2-adsorption–desorption isotherms of porous Co_3O_4 nanosheets (d) and Co_3O_4 nanorings (e). Squares = adsorption, inverted triangles = desorption. f) The first discharge curve of the Li–Co_3O_4 cells made by the as-prepared porous Co_3O_4 nanosheets (filled squares) and Co_3O_4 nanorings (empty circles) at a current density of 100 mA g^{-1}. Inset: cycle performance of the Li–Co_3O_4 cells at a current density of 100 mA g^{-1} at room temperature.

Figure 7a shows a typical TEM image of the porous Co_3O_4 nanosheets obtained by calcination of the as-prepared β-$Co(OH)_2$ nanosheets in air at 400 °C for 2 h. As with the β-$Co(OH)_2$ nanosheets, the porous Co_3O_4 nanosheets also consist of hexagonal and quasi-hexagonal structures with sizes ranging from 80 to 150 nm. However, under careful observation, the Co_3O_4 nanosheets were found to be composed of many pores with a mean diameter of 3 nm. The inset of Figure 7a is an SAED pattern taken from an individual Co_3O_4 nanosheet; the pattern consists of many spots, which shows that each porous Co_3O_4 nanosheet is a single crystal. All spots are identified as diffractions from spinel Co_3O_4. It is interesting that the as-prepared β-$Co(OH)_2$ nanosheets could be converted into Co_3O_4 nanorings by calcination in air at 600 °C for 2 h. A typical TEM image of the Co_3O_4 nanorings is shown in Figure 7b. It is clear that some of the Co_3O_4 nanocrystals exhibit ringlike structures with an average size of about 100 nm. The inset shows an SAED pattern taken from a mass of the Co_3O_4 nanorings; the pattern reveals the satisfactory crystallinity of the sample, which can be indexed to the face-centered-cubic phase of spinel Co_3O_4. A typical HRTEM image of an individual Co_3O_4 nanoring is shown in Figure 7c. The magnified image (inset) shows that the nanoring is structurally uniform with an interlayer spacing about 0.46 nm, which corresponds to the value of the (111) lattice plane of spinel Co_3O_4. The Brunauer–Emmett–Teller (BET) method with nitrogen adsorption was carried out to investigate the surface-area data of the as-prepared Co_3O_4 samples, which is critical for their technological application. The N_2-adsorption–desorption isotherm of the as-prepared Co_3O_4 can be categorized as type IV with a distinct hysteresis loop. The BET surface-area data was calculated to be about 18.153 $m^2 g^{-1}$ for the porous Co_3O_4 nanosheets (Figure 7d) and 13.734 $m^2 g^{-1}$ for the Co_3O_4 nanorings (Figure 7e).

Figure 7f shows the initial discharge curve and the cycle performance of the Li–Co_3O_4 cell made by the as-prepared Co_3O_4 at a current density of 100 mA g^{-1} at room temperature. The porous Co_3O_4 nanosheets had the most initial insertion capacity at 1301 mAh g^{-1}, and their capacity came to about 1011 mAh g^{-1} after the second cycle. Subsequently, the discharge capacity of the Li–Co_3O_4 cell appeared to increase slightly, which usually proceeds with the activation process for the electrochemical reaction of lithium. The as-prepared porous Co_3O_4 nanosheets exhibited excellent cyclability. After 21 cycles, the as-prepared porous Co_3O_4

CHEMISTRY
AN ASIAN JOURNAL

nanosheet electrode maintained a capacity of 1001 mAh g^{-1}, which corresponds to about 99% of the second discharge capacity. The initial capacity of the as-prepared Co_3O_4 nanorings reached 1298.7 mAh g^{-1}, whereas the capacity dropped rapidly to 676 mAh g^{-1} after 21 cycles. The capacity retention of the porous Co_3O_4 nanosheets was much better than that of the Co_3O_4 nanorings, which can be ascribed to the surface area and crystallinity of the samples. The porous Co_3O_4 nanosheets have a larger surface area and higher vacancy owing to poor crystallinity, which probably makes the lithium ions easy to extract and insert into the porous Co_3O_4 electrode and results in the increase in recharge ability.[30]

On the basis of the experimental results, a probable mechanism of formation of the hexagonal β-$Co(OH)_2$ nanosheets, porous Co_3O_4 nanosheets, and Co_3O_4 nanorings is proposed. The formation of the hexagonal β-$Co(OH)_2$ nanosheets may mainly comprise two processes: 1) formation of β-$Co(OH)_2$ crystal nuclei and 2) subsequent crystal growth from these nuclei to form hexagonal nanosheets. Triethylamine may play a key role in the crystal-growth process. Triethylamine was used both as an alkaline reagent to provide an alkaline environment and as a complexing reagent to influence the morphology of the final products. Our experimental results suggest that triethylamine may provide strong kinetic control over the growth rates of various faces of β-$Co(OH)_2$ by being selectively adsorbed on the crystal planes, which results in the formation of hexagonal β-$Co(OH)_2$ nanosheets.[31] However, it is still not clear how triethylamine influences the growth of the different crystal planes of β-$Co(OH)_2$. We also used diethanolamine and triethanolamine as alkaline and complexing reagents to prepare $Co(OH)_2$, but the morphology of the final products was irregular (see Supporting Information, Figures S3 and S4). The spinel Co_3O_4 nanorings may begin with the nanopores at the core of the hexagonal β-$Co(OH)_2$ nanosheets. The crystal structure of the hexagonal β-$Co(OH)_2$ nanosheets includes Co–OH layers and counter anions between the Co–OH layers. With elevated calcination temperature, the Co–OH layers are converted into cobalt oxide through pyrolysis and dehydration. Thus, the spaces of the OH layers and counter anions are converted into nanopores. With elongation of reaction time, the hexagonal β-$Co(OH)_2$ nanosheets gradually dehydrate and shrink and are finally converted into porous Co_3O_4 nanosheets and nanorings at different calcination temperatures.[32] The calcination temperature is especially important in the formation of Co_3O_4 nanorings. It is difficult to obtain Co_3O_4 nanorings at low calcination temperature, whereas the products of Co_3O_4 obtained at 400 °C for 2 h were mostly made up of nanosheets with porous structures. Hou et al.[15] also prepared porous Co_3O_4 nanosheets by thermal decomposition of hexagonal β-$Co(OH)_2$ nanosheets in air at 450 °C for 5 h. Our synthetic strategy could be employed to fabricate porous nanosheets and nanorings of other metal oxides by calcination of the corresponding metal hydroxide nanosheets under appropriate conditions.

Conclusions

In summary, we have developed a simple method for the synthesis of single-crystalline hexagonal β-$Co(OH)_2$ nanosheets in large quantities by choosing triethylamine as both an alkaline and a complexing reagent under mild conditions. This novel synthetic method can be carried out to synthesize other high-quality hydroxide nanosheets, and it should have potential applications in future large-scale syntheses owing to its high yield, simple reaction apparatus, and low reaction temperature. Notably, single-crystalline porous Co_3O_4 nanosheets and Co_3O_4 nanorings were selectively obtained by thermal decomposition of the single-crystalline β-$Co(OH)_2$ nanosheets in air at 400 and 600 °C, respectively, for 2 h. This strategy may become a general method for the fabrication of porous nanosheets and nanorings of other metal oxides by calcination of the corresponding metal hydroxide nanosheets under appropriate conditions.

Experimental Section

All chemicals used in this work, such as aqueous cobalt nitrate ($Co(NO_3)_2{\cdot}6H_2O$) and triethylamine, were analytical-grade reagents from the Beijing Chemical Factory, China. They were used without further purification.

Synthesis

In a typical procedure, $Co(NO_3)_2{\cdot}6H_2O$ (0.291 g, 1 mmol) was placed in a 50-mL teflon-lined autoclave and dissolved in deionized water (20 mL) to form a pink solution at room temperature. Triethylamine (0.5–1.5 mL) was then added dropwise with magnetic stirring, and the solution immediately turned black. Next, the autoclave was filled with deionized water up to 80% of the total volume and, after 10 min of stirring, sealed and maintained at 100–180 °C for 2–24 h without shaking or stirring. The resulting products were filtered and washed with deionized water and anhydrous ethanol several times, and finally dried under vacuum at 60 °C for 4 h. As-prepared cobalt hydroxide was calcined to produce porous nanosheets and nanorings of Co_3O_4 in air at 400–600 °C for 2 h.

Characterization

The samples obtained were characterized on a Brucker D8-advance powder X-ray diffractometer with $Cu_{K\alpha}$ radiation ($\lambda = 1.5418$ Å). The operation voltage and current were kept at 40 kV and 40 mA, respectively. The size and morphology of the as-synthesized products were determined at 20 kV by an XL30 S-FEG scanning electron microscope and at 160 kV by a JEM-200CX transmission electron microscope and a JEOL JEM-2010F high-resolution transmission electron microscope. SAED was further performed to determine the crystallinity. DSC and TGA were carried out with a NETZSCH STA-449C simultaneous TG-DTA/DSC apparatus at a heating rate of 10 K min^{-1} in flowing air. A nitrogen-adsorption system (Coulter SA 3100 plus) was employed to record the adsorption–desorption isotherm at the liquid-nitrogen temperature of 196 °C. The electrochemical properties of the as-prepared Co_3O_4 as cathode were evaluated by using two-electrode cells with lithium metal as anode. The cathode was prepared by compressing a mixture of Co_3O_4/acetylene black/polyvinylidene fluoride (PVDF) with a weight ratio 75:15:15. The cathode was dried for 24 h at 80 °C in a vacuum oven and cut into a disk (1.0 cm^2). The electrolyte solution was 1 M $LiPF_6$ dissolved in a 1:1 mixture of ethylene carbonate/diethyl carbonate. The cell was assembled in an Ar-filled glovebox with porous polypropylene (Celgard 2500) as a separator. The electrode capacity was measured by a galvanostatic charge/discharge experiment with a current density of 100 mA g^{-1} at a potential between 0 and 3.0 V.

Acknowledgements

Financial support of this work by the National Natural Science Foundation of China (No. 50504017), the Hunan Provincial Key Science and Technology Project of China (No. 2007FJ3008), and the Hunan Postdoctoral Scientific Program of China (No. 2006FJ4230) is gratefully acknowledged.

[1] a) Z. P. Xu, H. C. Zeng, *Chem. Mater.* **1999**, *11*, 67; b) P. V. Kamath, G. H. A. Therese, J. Gopalakrishnan, *J. Solid State Chem.* **1997**, *128*, 38.
[2] a) L. Cao, F. Xu, Y. Y. Liang, H. L. Li, *Adv. Mater.* **2004**, *16*, 1853; b) V. Pralong, A. Delahaye-Vidal, B. Beaudoin, J. B. Leriche, J. M. Tarascon, *J. Electrochem. Soc.* **2000**, *147*, 1306.
[3] L. Zhang, A. K. Dutta, G. Jarero, P. Stroeve, *Langmuir* **2000**, *16*, 7095.
[4] a) M. Butel, L. Gautier, C. Delmas, *Solid State Ionics* **1999**, *122*, 271; b) M. Oshitani, H. Yufu, K. Takashima, S. Tsuji, Y. Massumaru, *J. Electrochem. Soc.* **1989**, *136*, 1590.
[5] a) Ch. Mockenhaupt, Th. Zeiske, H. D. Lutz, *J. Mol. Struct.* **1998**, *443*, 191; b) P. Benson, G. W. D. Briggs, W. F. K. Wynne-Jones, *Electrochim. Acta* **1964**, *9*, 275.
[6] V. Pralong, A. Delahaye-Vidal, B. Beaudoin, B. Gérand, J.-M. Tarascon, *J. Mater. Chem.* **1999**, *9*, 955.
[7] a) F. Lichtenberg, K. Kleinsorgen, *J. Power Sources* **1996**, *62*, 207; b) K. Watanabe, T. Kikuoka, N. Kumagai, *J. Appl. Electrochem.* **1995**, *25*, 219.
[8] T. N. Ramesh, M. Rajamathi, P. V. Kamath, *Solid State Sci.* **2003**, *5*, 751.
[9] P. Elumalai, H. N. Vasan, N. Munichandraiah, *J. Power Sources* **2001**, *93*, 201.
[10] M. Dixit, G. N. Subbanna, P. V. Kamath, *J. Mater. Chem.* **1996**, *6*, 1429.
[11] R. S. Jayashree, P. Vishnu Kamath, *J. Mater. Chem.* **1999**, *9*, 961.
[12] J. T. Sampanthar, H. C. Zeng, *J. Am. Chem. Soc.* **2002**, *124*, 6668.
[13] X. L. Li, J. F. Liu, Y. D. Li, *Mater. Chem. Phys.* **2003**, *80*, 222.
[14] Z. Liu, R. Ma, M. Osada, K. Takada, T. Sasaki, *J. Am. Chem. Soc.* **2005**, *127*, 13869.
[15] Y. Hou, H. Kondoh, M. Shimojo, T. Kogure, T. Ohta, *J. Phys. Chem. B* **2005**, *109*, 19094.
[16] M. Andok, T. Kobayashi, S. Iijima, M. Haruta, *J. Mater. Chem.* **1997**, *7*, 1779.
[17] P. Nkeng, J. Koening, J. Gautier, P. Chartier, G. J. Poillerat, *Electroanal. Chem.* **1996**, *402*, 81.
[18] a) M. T. Verelst, O. Ely, C. Amiens, E. Snoeck, P. Lecante, A. Mosset, M. Respaud, J. M. Brotom, B. Chaudret, *Chem. Mater.* **1999**, *11*, 2702; b) S. Takada, M. Fujii, S. Kohiki, *Nano Lett.* **2001**, *1*, 379; c) S. A. Makhlouf, *J. Magn. Magn. Mater.* **2002**, *246*, 184.
[19] D. Barreca, C. Massignan, S. Daolio, M. Fabrizio, C. Piccirillo, L. Armelao, E. Tondello, *Chem. Mater.* **2001**, *13*, 588.
[20] M. E. Baydi, G. Poillerat, J.-L. Rehspringer, J. L. Gautier, J.-F. Koenig, P. Chartier, *J. Solid State Chem.* **1994**, *109*, 281.
[21] E. Fujii, H. Torii, A. Tomozawa, R. Takayama, T. Hirao, *J. Mater. Sci.* **1995**, *30*, 6013.
[22] J. L. Gautier, E. Rios, M. Gracia, J. F. Marco, J. R. Gancedo, *Thin Solid Films* **1997**, *311*, 51.
[23] E. Matijevic, *Chem. Mater.* **1993**, *5*, 412.
[24] T. He, D. R. Chen, X. L. Jiao, Y. L. Wang, *Adv. Mater.* **2006**, *18*, 1078.
[25] a) X. H. Liu, G. Z. Qiu, X. G. Li, *Nanotechnology* **2005**, *16*, 3035; b) R. Xu, H. C. Zeng, *Langmuir* **2004**, *20*, 9780; c) R. Xu, H. C. Zeng, *J. Phys. Chem. B* **2003**, *107*, 926; d) J. Feng, H. C. Zeng, *Chem. Mater.* **2003**, *15*, 2829.
[26] H. Guan, C. Shao, S. Wen, B. Chen, J. Gong, X. Yang, *Mater. Chem. Phys.* **2003**, *82*, 1002.
[27] Y. K. Liu, G. H. Wang, C. K. Xua, W. Z. Wang, *Chem. Commun.* **2002**,1486.
[28] X. Y. Shi, S. B. Han, R. J. Sanedrin, C. Galvez, D. G. Ho, B. Hernandez, F. M. Zhou, M. Selke, *Nano Lett.* **2002**, *2*, 289.
[29] X. M. Sun, Y. D. Li, *Chem. Commun.* **2003**, 1768.
[30] X. Wang, X. Y. Chen, L. S. Gao, H. G. Zheng, Z. D. Zhang, Y. T. Qian, *J. Phys. Chem. B* **2004**, *108*, 16401.
[31] X. P. Sun, S. J. Dong, E. K. Wang, *Langmuir* **2005**, *21*, 4710.
[32] a) X. H. Liu, G. Z. Qiu, Z. Wang, X. G. Li, *Nanotechnology* **2005**, *16*, 1400; b) E. Hosono, S. Fujihara; I. Honma, H. S. Zhou, *J. Mater. Chem.* **2005**, *15*, 1938.

Received: August 23, 2007
Revised: October 29, 2007
Published online: February 28, 2008

